COBEM 2021 26th International Congress of Mechanical Engineering
November 22-26, 2021, Virtual Congress, Brazil
ABCM Associação Brasileira de Engenharia e Ciências Mecânicas

COB-2021-1218
Numerical Investigation of Natural Gas Mixture Through a Supersonic Separator

Lucas de Souza Melo
João Victor Ota de Oliveira
Federal University of ABC, Alameda da Universidade, s/n - Anchieta, São Bernardo do Campo - SP, 09606-045
l.souza@aluno.ufabc.edu.br
joao.ota@aluno.ufabc.edu.br

Reinaldo Marcondes Orselli
Federal University of ABC, Alameda da Universidade, s/n - Anchieta, São Bernardo do Campo - SP, 09606-045
reinaldo.orselli@ufabc.edu.br

Ricardo Galdino da Silva
Institute of Aeronautics and Space, Praça Marechal Eduardo Gomes, nº 50, São José dos Campos - SP, 12228-970
ri_galdino@yahoo.com.br

Bruno Souza Carmo
Polytechnic School of University of São Paulo, Avenue Professor Luciano Gualberto, Travessa 3, 380 - Butantã, São Paulo, SP,Brazil
bruno.carmo@usp.br

Abstract. *Supersonic separators are devices used for separating heavier components of gas mixtures, usually applied for the process of natural gas extraction to separate high concentrations of CO_2. This technology is based on supersonic gas expansion allowing the condensation of some components mixed with the gas. Through centrifugation, the liquid droplets formed from condensation are carried towards the wall to be captured by attached collectors, thus, enabling the separation of the condensed component from the gas mixture. In this context, predicting and analyzing the gas flow behavior in the supersonic gas separator device is the main proposal of the present work, which is done by carrying out numerical simulations. The configuration considered for the numerical simulations is of an axisymmetric convergent-divergent nozzle with a collector and an outlet diffuser. At the inlet section, we impose a swirling flow which generates the centrifugation needed to separate the condensate. The numerical simulations are based on the Finite Volume Method, and, to numerically solve the turbulent flow, the flow governing equations with turbulence modeling (RANS equations) are considered. Attributes such as energy losses, swirl strength and shock wave position are analyzed.*

Keywords: *compressible flow, computational fluid dynamics, natural gas, shock wave, supersonic separator.*

1. INTRODUCTION

Oil and gas fields on the Brazilian coast, situated in the region known as the pre-salt layer, are one of the most important discoveries over the last few years in Brazil. When it comes to the exploration of natural gas in these fields, one of the challenges is the separation of heavier components, for example the carbon dioxide, that are extracted with it. As a way to make the separation viable on Offshore platforms, alternatives have been studied. Among them, there is the supersonic separator device, which is a new technology used to separate heavier components from gas mixtures (EPE, 2018).

This device is based on the supersonic expansion of the gas allowing the condensation of some components mixed with the gas. As it is energetically efficient and compact, it matches the Offshore application for which its development is intended. With this in perspective, the proposal to be developed in this study is to investigate, based on numerical simulations, the behavior of the flow of natural gas mixed when passing trrough a supersonic axisymmetric nozzle with a collector and the presence of a swirl generator. Features such as energy loss, amount of CO_2 removed in relation to the total in the process and collector geometry are analyzed. The computational code Ansys Fluent, based on the finite volume method, is used to perform the numerical simulations (Arinelli, 2015).

Nowadays, there are two main manufacturers of this type of device: Twister BV, which is a joint venture between Beacon Group and Shell, and ENGO (Twister BV, 2017; Imaev et al., 2014). The difference between the Twister's supersonic separator and the ENGO 3S (Fig. 1) is that the Twister's solution has a central body in it, that is not only used to produce swirl at the entrance of the device, but also change the nozzle profile, generating changes in the acceleration

profile. These geometries compose the state-of-the-art of this type of device. In this project, a research geometry that resembles an ENGO 3S device is used as presented in references Yang et al. (2014a) and Yang et al. (2014b).

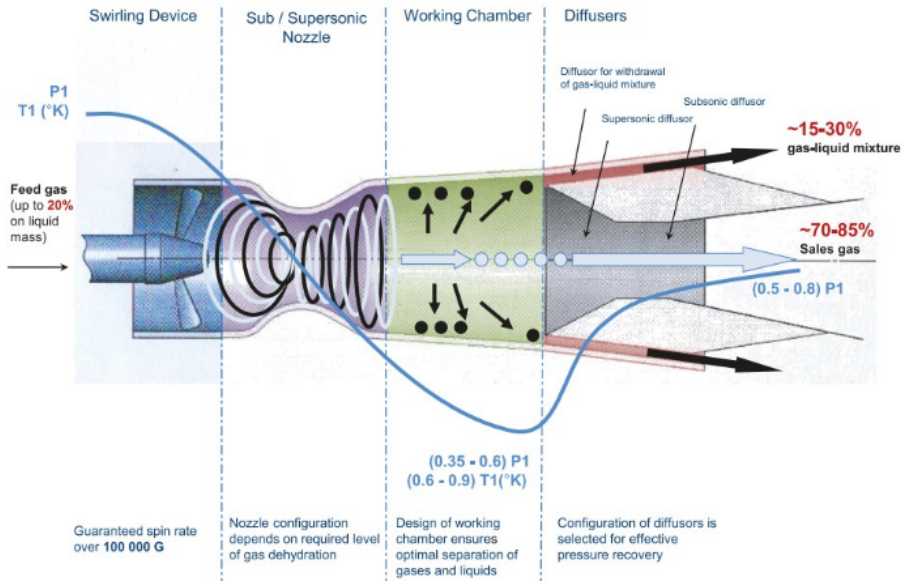

Figure 1. ENGO 3S supersonic separator. (Imaev et al., 2014).

The purpose of this work is to carry out numerical simulations to assess the capability of the numerical methodology to predict the flow behavior inside a supersonic convergent-divergent nozzle. The geometry used is based on the geometry available in the work of Yang et al. (2014a). This study was carried out in order to evaluate the energy loss when centrifugation is imposed, as well as relating with CO_2 ratio. The ANSYS Fluent commercial code, based on the finite volume method, is used to perform all numerical simulations (Ansys Inc, 2013).

2. METHODOLOGY

In order to investigate the different characteristics of the flow through a supersonic separator, with variations on the imposed swirl strength for two different turbulence models, a set of simulations are carried out using the same geometry and mesh for all the cases

The numerical discretization method is based on the finite volume method, in which the computational domain is divided in control volumes keeping mass, momentum and energy balance. To be solved numerically through iterations, they are converted to algebraic equations. This method has been widely used in various fields of engineering. A full description of the method can be found in Versteeg Malalasekera (2007). Numerical solution methodologies for compressible flow were used according to the descriptions made by Maliska (2004).

To avoid solving all turbulent fluctuating scales for high speed flow such as the supersonic separator, the RANS (Reynolds-Averaged Navier-Stokes) equations associated with turbulent models are used. Two turbulence models are considered in this investigation: k-ε RNG (Yakhot et al., 1992) and k-ω SST (Menter, 1992). Those models are available in ANSYS Fluent computational code (Ansys Inc, 2013).

2.1 Geometry and mesh

The nozzle geometry used for the numerical simulations, based in the work of Yang et al. (2014), is presented in Fig. 2. With respect to the work of Yang et al. (2014) that considered a planar nozzle, the geometry was adapted to be axisymmetric with the same area relations and same length.

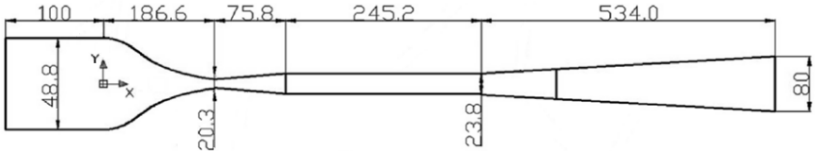

Figure 2. Dimensions in mm of the separator without the collector.

For the convergent region of the Laval nozzle of the geometry, its shape is described from the following equation:

$$\frac{D - D_{out}}{D_{cr} - D_{out}} = \frac{K_1}{(1 - x_m)^2}\left(1 - \frac{x}{L_{div,cub}}\right)^3 + \frac{K_2}{(1 - x_m)^2}\left(1 - \frac{x}{L_{div,cub}}\right)^2 \tag{1}$$

Where x is the axial distance between an arbitrary cross section and the inlet section, D is the convergent diameter at an arbitrary cross section of x, D_{in} is the inlet diameter, D_{cr} is the throat diameter and L_{conv} is the length of the convergent part of the nozzle. X_m is an arbitrary parameter chosen as X_m = 0.45. (Yang et al., 2014a). For the divergent region of the nozzle, the method of Foelsch (1949) is used. The first part is an arc of a circle of radius R = 743.314 mm and the second branch is obtained by the expression, where X_m = 0.45, K_1 = 0.322392, K_2 = 1.322392 and $L_{div,cub}$ = 45.48 mm. X_m, K_1 and K_2 are arbitrary parameters. $L_{div,cub}$ is the length of the divergent part of the nozzle.

$$\begin{cases} \frac{D-D_{cr}}{D_{in}-D_{cr}} = 1 - \frac{1}{x_m^2}\left(\frac{x}{L_{conv}}\right)^3 & \left(\frac{x}{L_{conv}} \leq x_m\right) \\ \frac{D-D_{cr}}{D_{in}-D_{cr}} = \frac{1}{(1-x_m)^2}\left(1 - \frac{x}{L_{conv}}\right)^3 & \left(\frac{x}{L_{conv}} \geq x_m\right) \end{cases} \tag{2}$$

The proposed model does not present the dimensions of the entrance and outlet area of the collector, as well as the inclination angle. A previous estimate is used for these parameters and is shown in Fig. 3.

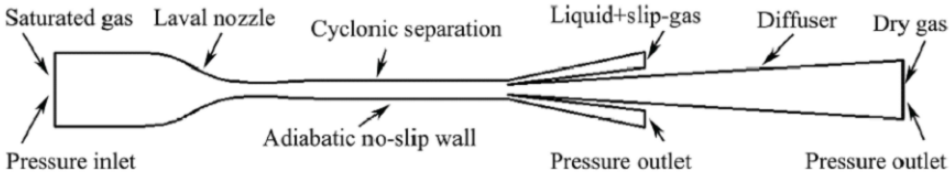

Figure 3. Geometry introduced by Yang et al. (2014).

The geometry (axisymmetric) with the collector is presented in Fig. 4, only half of the nozzle is shown due to symmetry along the axis. Thus, the dimensions of the collector are: h = 0.00478 m, collector outlet height Hout,collector = 0.01424 mm, collector entrance area $A_{collector}$ = 0.00028561 m^2. The cross-sectional area of the cyclonic section is $A_{cross-sectionRatio}$ = 0.000444881 m^2 and $A_{collector}$/ $A_{cross-sectionRatio}$ = 0.64. The cyclonic section is the region that starts upstream of the throat and ends at the entrance to the collector. In this region the flow is supersonic.

Figure 4. Geometry used for the numerical simulations, based on the work of Yang et al. (2014a).

The first computational mesh was generated with the commercial code ANSYS Mesh and consists of a total of 71782 volumes. As illustrated in Fig. 5 and 6, the mesh is structured, and refinement was made towards the wall to resolve the boundary layer as well around the corner at the junction between the collector and the main nozzle.

Figure 5. Near collector region view.

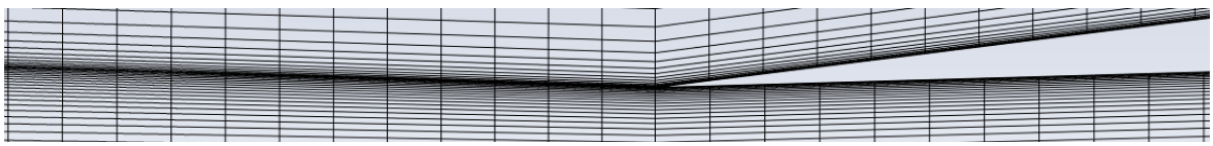

Figure 6. Collector intern wall refinement view.

In order to verify the grid sensitivity of the results, a grid-sensitivity analysis was performed by means of three grids: the main grid with 71782 cells, a fine grid with 106680 cells and a coarse grid with 45260 cells. As can be seen in Fig. 7 which contains the static pressure in the supersonic separator for the three different mesh refinements, the number of cells does not influence the accuracy of the simulation results by a significant amount.

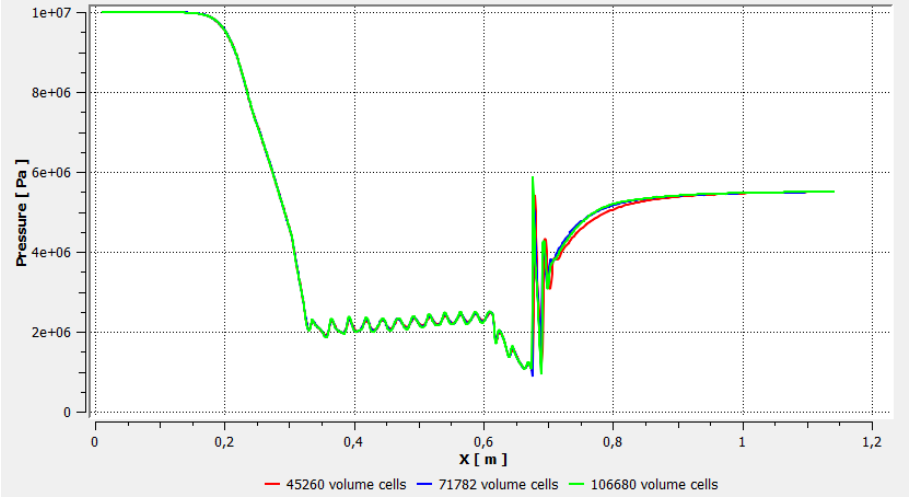

Figure 7. Static pressure variation along along the nozzle axis with three different mesh refinements.

2.2 Numerical setup

The boundary conditions of this work are the following: the inlet total pressure and total temperature are 100 bar and 288.47 K, respectively, due to the correlation with the work of Yang (2014). The outlet static pressure is 55 bar, which is set with respect to the position of the shock wave to occur just downstream the collector junction. The total temperature is the same as the inlet section, 288.47 K. All the walls are set as adiabatic, no-slip wall, and the asymmetric condition is applied to the axis line. The fluid is considered as a calorically perfect gas. It is ideal gas in the first simulations and real gas (Redlich-Kwong model) in the mixture simulation. The real gas Redlich-Kwong model (Redlich and Kwong, 1949) is an analytical cubic equation and widely used for having a relatively simple form, being one of the most widely validated equations for real gas simulation.

(Redlich and Kwong, 1949) is an analytic cubic equation of state with a relatively simple form. details about The pressure based solver as named in software the Ansys Fluent, which is the segregated solver as aforementioned, is used.

For the pressure velocity coupling associated with the segregated Pressure-based solver, there are some algorithms available to be chosen in Fluent, such as SIMPLE, SIMPLEC, among them, more recently, a new algorithm was implemented named as coupled. The fundamental difference between them is that in the classic segregated algorithm the governing equations are solved one after the other in a segregated manner, whereas in the coupled method they are solved at the same time by means of a system of equations . In this way, the Coupled scheme was used. (ANSYS Inc., 2013)

In terms of the spatial discretization, a second order upwind discretization scheme is applied for all the convective terms of the transport equations: density, momentum, turbulent kinetic energy, turbulent dissipation rate and energy. For computing the gradient, the Green-Gauss Node Based scheme is used. For the pressure parameter, the scheme PRESTO is used, which stands for Pressure Staggering Option and is an interpolation scheme based on a ‘staggered’ control volume arrangement, was used (Versteeg Malalaskera, 2007).

In this work, it is assumed a maximum value of 1e-6 for the residual of the energy transport equation and a maximum value of 1e-4 for all other transport equations. According to Ansys Inc (2013), a general reference to the numerical convergence criteria is the maximum residual value of 1e-6 for the energy transport equation and a maximum value of 1e-3 for all transport equations. In ANSYS Fluent, the residuals are calculated by the residual vector, also called imbalance, more details about the residuals definition are presented in Ansys Inc (2013) .

3. Results

3.1 Turbulence model k-ε RNG

The first turbulence model considered is k-ε RNG. In order to improve the solution of the flow gradients near the wall region a blended wall model is used. It is known as Enhanced Wall Treatment and it is a two layer model that carries a blend damping function that helps to make a smooth transition between the two layers (near wall model to viscous sublayer region, based on the logarithmic law). As well, the options of the k-ε RNG implemented in Fluent, the Pressure Gradient Effects, Compressibility Effects, Thermal Effects and Viscous Heating effect were activated, the options are described in Ansys Inc (2013). To verify the swirl’s influence in the results, two simulations are carried out: a standard simulation without swirl and a 5 degrees theta swirl generation simulation. Theta is the angle of the velocity imposed at the inlet. It is given by the tangent of the relation between axial mean velocity and tangential mean velocity. Only the

tangent velocity vector of the swirl (in relation to the axial velocity) is fixed at the nozzle inlet. For the k-ε simulations, the residuals values (for a compatible number of iterations) are presented in Tab. 1. Both simulations reached a lower residual value according to the criteria set as aforementioned.

Table 1. Residual values for each transport equation with the k-ε RNG model

Case	Continuity	x-velocity	y-velocity	Swirl	Energy	k	ε
k- RNG no swirl	3.0583e-06	2.7343e-09	7.6471e-10	-	3.8502e-10	4.3026e-09	1.3966e-08
k- RNG 5° swirl	2.6049e-07	6.9782e-10	7.7622e-11	8.9259e-10	8.9433e-11	8.9433e-11	9.2428e-10

The curves of the static pressure and Mach number along the nozzle axis obtained from both cases are compared as shown in Fig. 8. The cases show a difference in the values when compared in terms of static pressure and Mach number which is expected, once that an additional radial velocity is imposed at the inlet in the 5° swirl case.

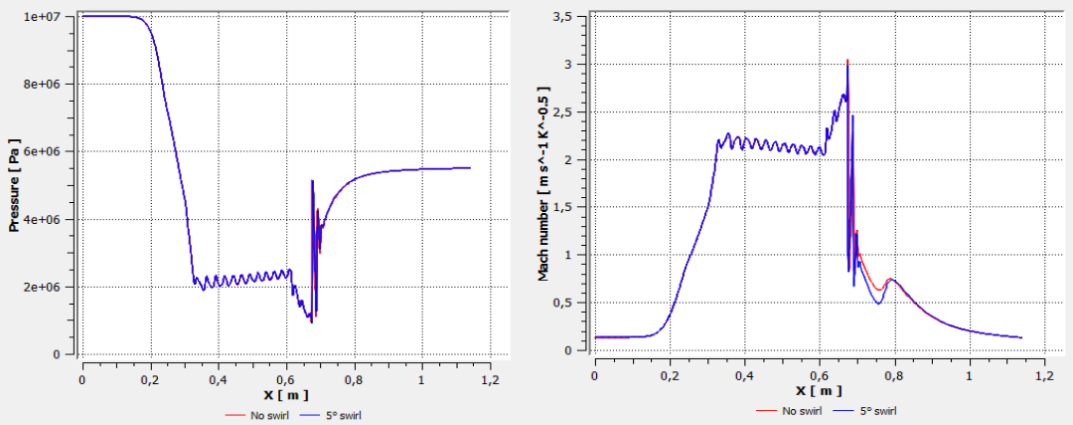

Figure 8. Static pressure (left) and Mach number (right) at the axis for k- RNG. Red line: no swirl; blue line: 5º swirl.

For both of the simulations the y plus (y+), the nondimensional wall distance of the first cell adjacent to the wall, (the definition of this parameter is available in the reference Versteeg Malalasekera, 2007) presented a range of values from 1 to 300 along the separator. The used y plus maximum value of 300 agrees with the considered limit within the logarithmic region of the boundary layer. This region of the boundary layer is known as "log-law layer" and is a turbulent region where (Reynolds) turbulent stress predominates in the flow. In Fig. 8 it is possible to see that to the shock wave region of the collector the maximum static pressure value of the 5° swirl simulation is higher when compared to the no swirl simulation, as well as the minimum Mach number value of the 5° swirl simulation is lower when compared to the no swirl simulation. Subtracting the values of Mach number between both of the simulations to each point of the domain, in the majority of the near collector region, the Mach number value is slightly higher in the 5° swirl simulation, when compared to the no swirl simulation. That occurs as a result of the radial velocity inputted by the swirl, which turns on acceleration to the fluid in that region. At the shock wave region, the Mach number value is lower in the 5° swirl simulation, when compared to the no swirl simulation, which indicates that the swirl case generates a stronger shock (higher static pressure), generated by the higher velocity.

3.2 Turbulence model k-ω SST

The second turbulence model considered is the k-ω SST, with the following options available in ANSYS Fluent (see Ansys Inc, 2013) set on: compressibility Effects, Viscous Heating effect and Production Limiter. Its results are compared with the corresponding ones provided by the k-ε RNG model. To verify the influence of the swirl in the results, two simulations are carried out: a standard simulation without swirl and a 5 degrees theta swirl simulation. For the k-ω SST simulations, the residual values are presented in Tab. 2. Likewise, with both simulations, the residual values reached values below the criteria as aforementioned (1e-4 for all transport equations, except energy equations set as 1e-6) .

Table 2. Residual values for each transport equation with the k-ω SST model

Case	Continuity	x-velocity	y-velocity	Swirl	Energy	k	ε
k- RNG no swirl	4.6733e-07	8.1859e-10	1.9324e-10	-	1.1185e-10	2.4561e-09	6.2708e-10
k- RNG 5° swirl	4.9319e-08	9.4922e-11	1.3050e-11	5.1098e-11	1.3544e-11	1.4020e-10	8.2406e-11

For both of the simulations the y plus presented a range of values from 1 to 300 along the separator, as in the k-ε RNG

cases. In the same way as in the k-ε RNG cases, in the majority of the near collector region the Mach number value is slightly higher in the 5° swirl simulation when compared to the no swirl simulation, as well as in the shock wave region the Mach number value is lower in the 5° swirl simulation when compared to the no swirl simulation.

The curves of the static pressure and Mach number along the nozzle axis obtained from both cases with and without swirl are compared as shown in Fig. 9. This case follows the same pattern as observed with k-ε: the cases show a difference in the values when compared in terms of pressure and Mach number. In Fig. 9 it is possible to see that to the shock wave region of the collector and to the central body the maximum value of the 5° swirl static pressure is higher and the minimum of 5° swirl velocity is lower when compared to the no swirl simulation. However, in this case the difference between the 5 degree swirl simulation and the no swirl simulation is barely noticed when compared with the difference observed with k-ε. Simulations with stronger swirl intensity are in progress so that the difference should be more noticeable.

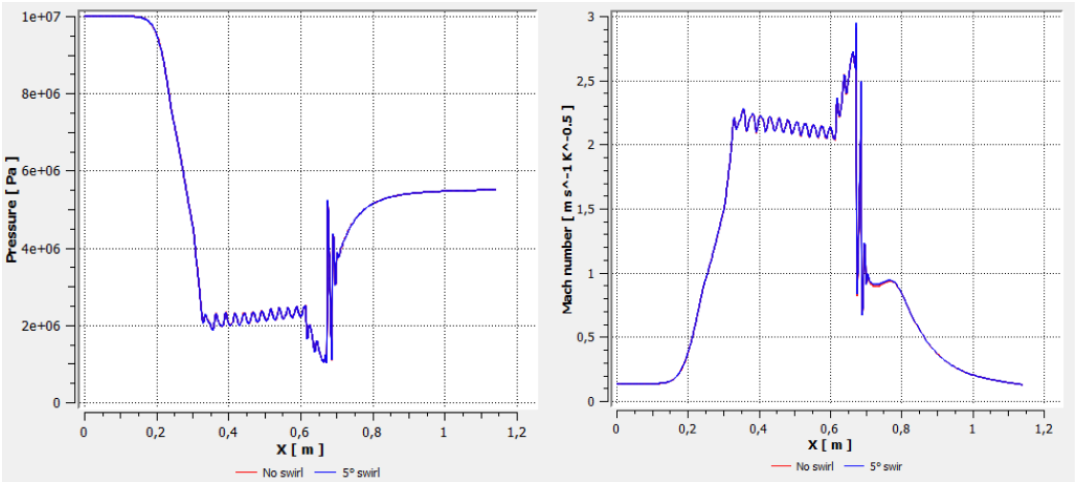

Figure 9. Static pressure (left) and Mach number (right) at the axis for k-ω SST. Red line: no swirl; blue line: 5º swirl.

3.3 Comparisons of the results between k-ε RNG and k-ω SST

Figure 10 shows the no swirl k-ε RNG when compared with the no swirl k-ω SST and the 5° swirl k-ε RNG when compared to the 5° swirl k-ω SST. Based on the results presented in Fig. 8, 9 and 10, it is possible to conclude that the results showed with both models are very similar to each other.

As such, with respect to the turbulence model used, at least for these two models, the results obtained were not affected significantly in terms of main variables presented of the static pressure and Mach number variation along the nozzle, as well as its shock wave position. In addition, for the cases with swirl, the results presented with both turbulence models were also in very good agreement. Such observations indicate that the choice of the turbulence models, at least for these two which are commonly used in the literature, is not so important for the analyzes of the flow behavior through the supersonic nozzle as with the axisymmetric geometry proposed for this work.

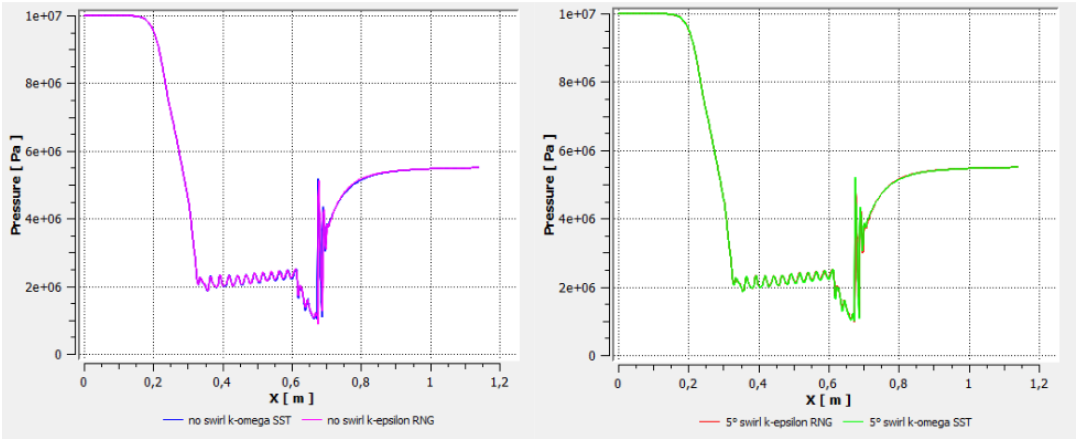

Figure 10. Comparison between k-ε RNG and k-ω SST with the curves of Static pressure. Left: no swirl; right: 5º swirl.

3.4 θ = 35° swirl simulation

As seen when comparing the two turbulence models (Fig. 8, 9 and 10), the results are very similar between both, and for this reason, only the k-ε RNG model was considered in the simulations carried out for the swirl with θ = 35° simulation presented in this section. In addition to the simulations presented in the previous sections, the real gas model Redlich-Kwong was used along with axial velocity and tangential velocity profiles imposed at the inlet, resulting in the swirl with θ = 35°. The real gas model Redlich-Kwong is commonly used as the real gas model, as can be seen in the reference Yang et al. (2014a).

The profile used was based on the swirl velocity of a previous simulation. It was taken from 0.1 meters downstream from the inlet. This profile was selected to be imposed at the inlet because it represents a proper and coherent development of the flow. Figure 11 shows the profile imposed at the inlet.

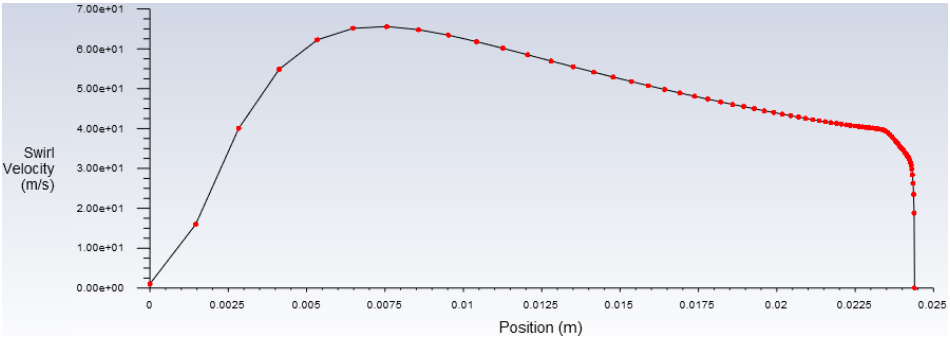

Figure 11. Velocity profile imposed at the inlet

Observing Fig. 11, it can be noticed that the profile goes to zero on both sides. The near wall zero value due to the effects of the boundary layer, while the near axis zero is due to the definition of the velocity gradient in the symmetric region which need to be zero, once it is given by:

$$\frac{\partial p}{\partial r} = \frac{\rho V_\theta^2}{r} \tag{3}$$

Where V_θ is the tangential velocity and r is the radial coordinate in relation to the axis. The residuals values of the simulations are presented in Table 3. The simulations did not reach the lower residual value according to the criteria set as aforementioned yet. Once that is a preliminary result that does not fulfill the aim of the research project completely, it was considered acceptable and by its analysis, coherent. Additional strategies to reduce the residuals are in progress. The residual values for the simulations are presented in Tab. 3.

Table 3. Residual values for each transport equation for k-ε RNG 35° swirl and k-ε RNG 5° swirl

Case	Continuity	x-velocity	y-velocity	Swirl	Energy	k	ε
k-ε RNG 5° swirl	2.6049e-07	6.9782e-10	7.7622e-11	8.9259e-10	8.9433e-11	8.9433e-11	9.2428e-10
k-ε RNG 35° swirl	2.1952e-02	2.0454e-05	6.0057e-06	1.0459e-05	1.9695e-06	5.8025e-05	2.9319e-04

Figure 12 shows the curves of the static pressure and Mach number along the nozzle axis obtained from the cases when compared to each other. As can be seen, the 35° swirl simulation presents an alteration on the inlet pressure and outlet pressure when compared to the imposed pressures defined by the boundary conditions, while the 5° swirl simulation do not present this effect. This effect is due to the tangent velocity profile imposed in this case which alter the boundary conditions. This effect also occurs in the Mach number. The 5° swirl simulation reached a higher peak in terms of static pressure while the 35° swirl simulation reached a higher peak in terms of Mach Number.

For the θ = 35° simulation, the y plus, the nondimensional wall distance of the first cell adjacent to the wall, presented a range of values from 1 to 350 along the separator. Comparing this value with the maximum value of 300 of the 5° swirl simulation, it is 16.6% higher.

The increase of the centrifugal force in the region near the collector is the reason for the imposition of the swirl flow. Once that the flow is accelerated by the convergent-divergent region and, as a consequence, the heavier components condense due to the decrease of the temperature related to this acceleration, a high centrifugal force on the collector region lead those heavier components to be pushed towards the nozzle upper wall and be collected.

In the case simulated, the divergent section of the nozzle presents a 190,000 g (where g is the gravity acceleration), its higher value, while in the collector region of the nozzle the value presented is 110,000 g. In fact the best optimized

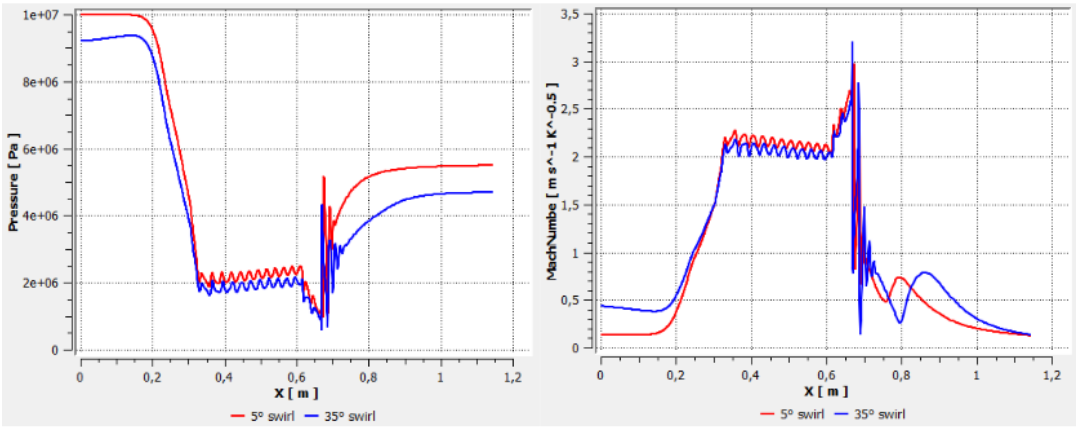

Figure 12. Static pressure (left) and Mach number (right) at the axis for 35° swirl and 5° swirl. Red line: 5° swirl; blue line: 35° swirl.

configuration to the distribution of the centrifugal acceleration is when the higher value of centrifugal acceleration is in the collector region, but given the geometry and the simulation parameters, the energy dissipation through the separator decreases it. Despite the not optimized distribution of the centrifugal force, when compared to the 5° swirl case which presents a 10,000 g centrifugal force in the collector region, the 35° swirl was responsible for a eleven times improvement in this parameter. However, according to the Brouwer and Epsom (2003), the order of the centrifugal acceleration in a real supersonic separator is at least 300,000 g - centrifugal acceleration strength in which it reaches an appropriate rate of separation. Figure 13 shows the contours of the centrifugal force through the supersonic separator. The radial direction of the figure is oversized to generate a better visualization. The scale is in g (gravity acceleration).

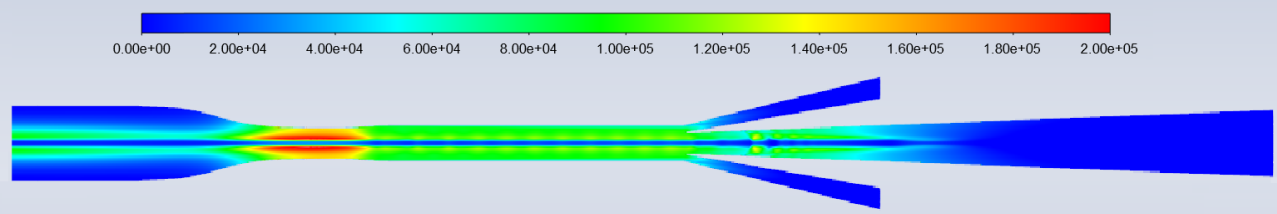

Figure 13. Centrifugal acceleration field in the single component simulation with swirl $\theta = 35°$.

Thus, additional work is necessary to improve the simulation convergence in order to be able to carry out additional simulations with higher values of swirl degree θ, axial velocity and lower back pressure to increase the centrifugal acceleration value.

3.5 No swirl CH_4-CO_2 mixture and 35° swirl CH_4-CO_2 mixture

As previously mentioned, when comparing the two turbulence models (Fig. 8, 9 and 10), the results are very similar between both, and for this reason, only the k-ε RNG model was considered in the simulations carried out for the no swirl multicomponent mixture of CH_4 /CO_2 and $\theta = 35°$ swirl multicomponent mixture of CH_4 /CO_2 presented in this section. The CO_2 concentration used in the mixture was 30%. The same profile used in the previous section (Fig. 11) is used in these simulations.

Along with the last section results, the simulations did not reach the lower residual value according to the criteria set as aforementioned yet. Once that is a preliminary result that does not fulfill the aim of the research project completely, it was considered acceptable and by its analysis, coherent. Additional strategies to reduce the residuals are in progress. The residual values for the simulations in this section are presented in Tab. 4.

Table 4. Residual values for each transport equation for multicomponent 35° swirl and multicomponent no swirl

Case	Continuity	x-velocity	y-velocity	Swirl	Energy	k	ε
Multicomp. no swirl	9.0824e-04	1.2597e-06	3.4270e-07	-	1.2281e-07	2.9666e-06	9.8859e-06
Multicomp. 35° swirl	2.7433e-02	4.4156e-06	1.4862e-06	1.2365e-05	8.5279e-06	4.4549e-05	2.5503e-04

Figure 14 shows the curves of the static pressure and Mach number along the nozzle axis obtained from the cases when compared to each other. As in the previous case, the 35° swirl simulation presents an alteration on the inlet pressure and

outlet pressure when compared to the imposed pressures defined by the boundary conditions, while the no swirl simulation do not. As aforementioned, this effect is due to the tangent velocity profile imposed in this case which alter the boundary conditions. This effect also occurs in the Mach number. Comparing the cases in terms of shock wave position, in the 35° swirl case it occurs earlier, less inside of the collector than the shock wave of the no swirl case. It is important that the shock occur just downstream the collector junction to enable the maximum energy conservation through the supersonic separator up to this point (and carry that condition as far as possible inside the collector), once that centrifugal forces of at least 300,000 g are necessary to achieve an appropriate rate of separation.

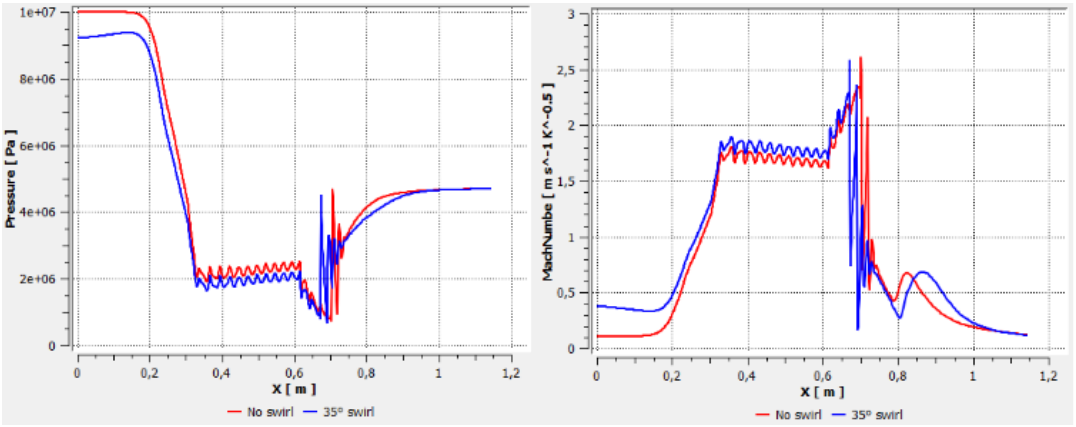

Figure 14. Static pressure (left) and Mach number (right) at the axis for 35° swirl and no swirl. Red line: No swirl; blue line: 35º swirl.

For the $\theta = 35°$ simulation, the y plus, the nondimensional wall distance of the first cell adjacent to the wall, presented a range of values from 1 to 225 along the separator. The no swirl simulation presented a range of values from 1 to 200 along the separator. Comparing the values between both simulations, the 35° swirl simulation has an increase of 12,5% in relation to the no swirl simulation. Both of them agree with the considered limit within the logarithmic region of the boundary layer.

In the 35° swirl case, the divergent section of the nozzle presents a 160,000 g, its higher value, while in the collector region of the nozzle the value presented is 90,000 g. The multicomponent 35° simulation showed a 18% decrease in terms of swirl strength in the collector region when compared to the single component 35° swirl simulation. As said, the best optimized configuration to the distribution of the centrifugal acceleration is when the higher value of centrifugal acceleration is in the collector region and in order to achieve that additional simulations with higher values of swirl degree θ, axial velocity and lower back pressure are necessary. Figure 15 shows the contours of the centrifugal force through the supersonic separator. The radial direction of the figure is oversized to generate a better visualization. The scale is in g (gravity acceleration).

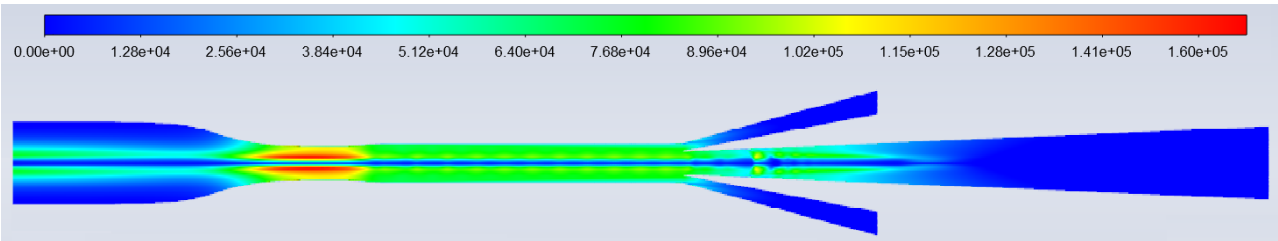

Figure 15. Centrifugal acceleration field in the multicomponent simulation with swirl $\theta = 35º$.

4. CONCLUSION

For the numerical data used in this investigation the k-ω SST model and k-ε RNG behaved similarly when compared in terms of static pressure and Mach number. For the generated data, the k-ω SST model showed a smoother growth behavior in terms of Mach number, when compared with k-ε RNG when a swirl is imposed at the inlet of the supersonic separator.

An analysis of the flow behavior for the simulated cases with and without swirl for the two turbulence models k-ε RNG and k-ω SST were presented. For the cases without swirl and with swirl, when comparing the results between the k-ε RNG and k-ω SST, the difference observed for the Mach number and Static pressure as well as the shock position were not affected significantly. For the cases with swirl, the results presented with both turbulence models were also in

good agreement.

As seen when comparing the two turbulence models (Fig. 8, 9 and 10), the results are very similar between both, and for this reason, only the k-ε RNG model was considered in the simulations carried out, which include the increase of the swirl degree θ = 35° in order to maximize its influence in the velocity profile, along with the inclusion of the 30% CO_2 / 70% CH_4 mixture. The swirl degree θ = 35° was achieved by the imposition of a velocity profile modification at the inlet, increasing the flow tangential velocity and decreasing both inlet and outlet static pressure.

The single component 35° swirl simulation showed an eleven times improvement in terms of swirl strength in the collector region in relation to the 5° swirl simulation. The multicomponent simulation 35° swirl simulation showed a 18% decrease in terms of swirl strength in the collector region when compared to the single component 35° swirl simulation. Once that is a preliminary result that does not fulfill the aim of the research project, additional simulations with higher values of swirl degree θ, axial velocity and lower back pressure in order to increase the centrifugal acceleration value are being carried out.

5. ACKNOWLEDGEMENTS

We wish to acknowledge the support provided by UFABC – Federal University of ABC sponsored by CNPq – National Council for Scientific and Technological Development (23006.001565/2020-10). We gratefully acknowledge support of the RCGI – Research Centre for Gas Innovation, hosted by the University of São Paulo (USP) and sponsored by FAPESP – São Paulo Research Foundation (2014/50279-4) and Shell Brasil, and the strategic importance of the support given by ANP (Brazil's National Oil, Natural Gas and Biofuels Agency) through the RD levy regulation.

6. REFERENCES

Ansys Inc., 2013. Fluent User Guide. https://www.ansys.com. Accessed 17 June 2021.

Arinelli, L.O., Medeiros, J.L., Araújo, O.Q., 2015. Performance analysis and comparison of membrane permeation versus supersonic separator for CO_2. Removal from a plausible natural gas of Libra field, Brazil, Offshore technology conference, OTC-26164-MS, Rio de Janeiro-RJ, 27-29

Brouwer, J.M. and Epsom, H.D., 2003. "Twister Supersonic Gas Conditioning for Unmanned Platforms and Subsea Gas Processing". Offshore Europe held in Aberdeen. UK, 2 -5 September 2003.

Energy Research Office - EPE, 2018. Desafios do Pré-Sal. https://www.epe.gov.br/sites-pt/publicacoes-dados-abertos/publicacoes/PublicacoesArquivos/publicacao-227/topico-457/Desafios%20do%20Pre-Sal.pdf.2021. Accessed 17 June

Foelsch, K., 1949. The Analytical Design of an Axially Symmetric Laval Nozzle for a Parallel and Uniform Jet, Journal of the Aeronautical Sciences.

Imaev, S.Z.; Bagirov L.A.; Borisov V.E.; Voytenko E.V. New low temperature process of CO_2 recovery from natural gases, SPE 171427, SPE Asia Pacific Oil Gas Conference and Exhibition, ENGO Engineering, Ltd, Adelaide, Australia.

Maliska C., 2004. Transferência de calor e mecânica dos fluidos computacional. 2nd edition, LTC (in portuguese).

Menter F.R., 1994. "Two-Equation Eddy-Viscosity Turbulence Models for Engineering Applications". AIAA Journal, 32 (8), 1598-1605.

Twister, Supersonic Gas Solutions., 2017. Twister supersonic separator - How it works. https://www.twisterbv.com/twister-supersonic/. 17 June 2021.

Vesteeg, H. K. and Malalasekera,W., 2007. An introduction to computational fluid dynamics - the finite volume method. [S.l.]:Addison-Wesley-Longman.

Yakhot V., Orszag S.A., Thangam S., Gatski T.B. Speziale C.G., 1992. Development of turbulence models for shear flows by a double expansion technique, Physics of Fluids A, Vol. 4, No. 7, pp. 1510-1520

Yang, Y., Wen, C. Wang, S. Feng, Y., 2014a. Numerical simulation of real gas flows in natural gas supersonic separation process, Journal of Natural Gas Science and Engineering 21, Elsevier.

Yang, Y., Wen, C. Wang, S. Feng, Y., 2014b. Effect of inlet and outlet flow conditions on natural gas parameters in supersonic separation process, PLOS ONE.

7. RESPONSIBILITY NOTICE

The authors are the only responsible for the printed material included in this paper.